Effects of stable stratification on turbulent/nonturbulent interfaces in turbulent mixing layers

T. Watanabe,[1,*] J. J. Riley,[2] and K. Nagata[1]

[1]*Department of Aerospace Engineering, Nagoya University, Nagoya, Japan*
[2]*Department of Mechanical Engineering, University of Washington, Seattle, USA*

(Received 23 January 2016; published 1 August 2016)

Direct numerical simulations are used for investigating the effects of stable stratification on the turbulent/nonturbulent (T/NT) interface in stably stratified mixing layers whose buoyancy Reynolds number Re_b on the centerline is large enough for small-scale three-dimensional turbulence to exist. The stratification changes the interface geometry, and a large part of the interface is oriented with normal in the vertical direction in the stratified flows. The structures of the T/NT interface layer are similar between the nonstratified and stratified flows, and the T/NT interface consists of the viscous superlayer and the turbulent sublayer. The stratification is locally strengthened near the T/NT interface as evidenced by the large vertical density gradient, resulting in the decrease in Re_b in the T/NT interface layer. Thus, even the small-scale dissipation range is directly affected by the buoyancy near the T/NT interface, although the small scales are somewhat free from the direct effects of the buoyancy in the turbulent core region. The production rates of enstrophy and scalar dissipation, which arise from the strain/vorticity and strain/density-gradient interactions, are decreased near the T/NT interface because the stratification modifies the alignments among the vorticity, density gradient, and strain-rate eigenvectors near the T/NT interface. This influence on the small-scale turbulence dynamics is not observed in the turbulent core region because of the large Re_b. A possible explanation is given for the influence of buoyancy on the alignment statistics based on the suppression of the vertical turbulent motions by buoyancy.

DOI: 10.1103/PhysRevFluids.1.044301

I. INTRODUCTION

Observations in the atmosphere and oceans have indicated that flows are often strongly stably stratified. Even under stably stratified conditions, shear motions generate turbulence, such as in ocean mixing layers [1] and atmospheric boundary layers [2]. Turbulence in the environment usually appears surrounded by laminar (or weakly turbulent) flows. Internal gravity wave breakdown can also result in the generation of turbulent patches in the stratified environment [3]. Therefore, an interface between turbulent and nonturbulent flows, the so-called turbulent/nonturbulent interface, exists in these flows. This interfacial region is responsible for the exchanges of mass, energy, momentum, and scalars between the turbulent and nonturbulent flows and governs the development of turbulent flows.

Turbulent/nonturbulent (T/NT) interfaces have been studied in nonstratified flows, especially in canonical flows such as mixing layers, jets, and boundary layers, and these studies are summarized in the recent review paper [4]. The T/NT interface was found to be a layer with finite thickness consisting of two inner layers [5]. Corrsin and Kistler [6] proposed that a very thin layer, where the viscous diffusion of vorticity causes the spreading of turbulent flows, exists at the edge of the turbulence. This layer is called the viscous superlayer and has indeed been observed at the outer edge by others [7,8]. Additionally, between the viscous superlayer and the turbulent core region, an adjacent layer called the turbulent sublayer was also found; here the vorticity is matched between the turbulent and nonturbulent flows [9]. The vorticity dynamics changes depending on these two layers: Nonturbulent fluids acquire vorticity in the viscous superlayer owing to viscous diffusion, while

*watanabe.tomoaki@c.nagoya-u.jp

inviscid vortex stretching has an important contribution in the turbulent sublayer [10]. Furthermore, studies of the T/NT interface showed that the turbulent entrainment process is dominated by the viscous diffusion of vorticity across the interface rather than by inviscid large-scale engulfment motions [7,11]. The T/NT interface is recently becoming better understood by high-resolution direct numerical simulations (DNS) [9] and experimental measurements based on particle image velocimetry [12]. And while the T/NT interface often appears in stratified flows in the environment, it has not been as well studied. Krug *et al.* [13] experimentally investigated the T/NT interface in gravity currents [14]. They showed that the stable stratification reduces the entrainment rate by changing the surface area of the T/NT interface.

In this paper an investigation is reported of the effects of the stable stratification on the T/NT interface; the research is based on the DNS of temporally evolving, stably stratified mixing layers. The turbulence is generated by the Kelvin-Helmholtz (KH) instability, which is one of the important sources of turbulence in the atmosphere and oceans [15]. We consider the case where the stratification is localized in the shear layer rather than the uniform stratification. This flow configuration is simple but is sometimes a good approximation of geophysical flows [16]. The development of this flow was discussed in detail by Smyth and Moum [17]. The turbulence is generated by the KH instability, the buoyancy begins to suppress the large-scale motions of the turbulence, and finally the fluid motions from large to small scales are strongly affected by the buoyancy. We focus on the second stage where the three-dimensional turbulence exists in the mixing layer while the large-scale motions are affected by the buoyancy.

The influence of the stratification near the T/NT interface is considered in this study with particular attention to small-scale turbulence dynamics. The strain-rate tensor S_{ij} and vorticity ω_i play an important role in the small-scale dynamics of turbulence [18]. The interaction between vorticity and strain leads to vortex stretching $\omega_i S_{ij}$ (or compression depending on the sign), and in turn to enstrophy production, as seen by the enstrophy production term in the enstrophy equation. In stratified flows, the scalar gradient $G_i = \partial\theta/\partial x_i$ (where θ is proportional to the density, as defined below) affects the vorticity through the generation of baroclinic torque. The strain-rate field also has an impact on the scalar gradient via the straining term $-G_i S_{ij}$. The complex interactions among ω_i, S_{ij}, and G_i were studied in homogeneous sheared turbulence with uniform stable stratification [19]. In nonstratified flows, the strain-rate tensor is sensitive to the large-scale fluid motions near the T/NT interface [20]. Therefore, we examine the small-scale dynamics related to the strain-rate tensor near the T/NT interface described by the strain/vorticity and strain/scalar-gradient interactions. The strain-rate tensor has three eigenvalues, denoted by s_1, s_2, and s_3 and ranging from largest to smallest ($s_1 \geqslant s_2 \geqslant s_3$); the corresponding eigenvectors are $\boldsymbol{e}_1$, $\boldsymbol{e}_2$, and $\boldsymbol{e}_3$. Because of incompressibility, $s_1 + s_2 + s_3 = 0, s_1 > 0$ (expansion) and $s_3 < 0$ (compression) while the intermediate eigenvalue s_2 can be either positive or negative. The production terms for the enstrophy ($\omega^2/2$) and scalar-dissipation rate ($\kappa G^2, \kappa$: the diffusivity coefficient) can be written in terms of s_i and $\boldsymbol{e}_i$ [18]:

$$\omega_i S_{ij} \omega_j = \omega^2 s_i (\boldsymbol{e}_i \cdot \hat{\boldsymbol{\omega}})^2, \tag{1}$$

$$-G_i S_{ij} G_j = -G^2 s_i (\hat{\boldsymbol{G}} \cdot \boldsymbol{e}_i)^2, \tag{2}$$

where $\hat{\boldsymbol{\omega}} = \boldsymbol{\omega}/|\boldsymbol{\omega}|$ and $\hat{\boldsymbol{G}} = \boldsymbol{G}/|\boldsymbol{G}|$ are the unit vorticity and scalar-gradient vectors. These inviscid terms become important in the turbulent sublayer, while they have much smaller contributions in the viscous superlayer than the viscous and molecular diffusion terms have [8]. Equations (1) and (2) imply the importance of the geometrical properties of the vectors. Various studies have shown that in nonstratified turbulence the alignment statistics among these vectors are highly universal: The vorticity tends to be parallel and perpendicular to the intermediate eigenvector $\boldsymbol{e}_2$ and the compressive eigenvector $\boldsymbol{e}_3$, respectively, while the scalar gradient preferentially aligns with $\boldsymbol{e}_3$ [21–23].

One of the important nondimensional numbers in stratified turbulence is the buoyancy Reynolds number $\mathrm{Re}_b = (L_O/\eta)^{4/3}$, where L_O is the Ozmidov scale and η is the Kolmogorov scale. The Kolmogorov scale is the smallest scale of turbulence while the Ozmidov scale is often interpreted as the smallest scale influenced by the buoyancy: Thus the scales larger than L_O are strongly affected by the buoyancy. When Re_b is small, three-dimensional turbulence cannot exist [24] since even the small-scale motions are suppressed by buoyancy, which acts down to the Kolmogorov scale. It has been shown that when Re_b is large enough, the turbulence dynamics at the small scales are quite similar between the nonstratified and stratified flows [25]. In this paper we will show that even if Re_b is large enough for three-dimensional turbulence to exist in the mixing layer, buoyancy still exerts significant influence on the small scales near the T/NT interface.

The paper is organized as follows. In Sec. II, we describe the numerical model of the stratified mixing layer and the numerical methods. The fundamental properties of the flow, such as the characteristic length scales, are presented in Sec. III. The characteristics of the T/NT interface are shown in Sec. IV, and the buoyancy effects on the small-scale turbulence are discussed in Sec. V. Finally, Sec. VI summarizes the conclusions.

II. GOVERNING EQUATIONS, NUMERICAL METHODS, AND COMPUTATIONAL PARAMETERS

Temporally evolving mixing layers in a stably stratified environment [25–27] are computed by the DNS of the Navier-Stokes equations within the Boussinesq approximation. The governing equations are the continuity equation, the moment equation, and transport equation for the scalar θ, which are written as follows:

$$\nabla \cdot \boldsymbol{U} = 0, \tag{3}$$

$$\frac{\partial \boldsymbol{U}}{\partial t} + (\boldsymbol{U} \cdot \nabla)\boldsymbol{U} = -\nabla(p/\rho_0) + \nu\nabla^2\boldsymbol{U} + g\theta\boldsymbol{e}_y, \tag{4}$$

$$\frac{\partial \theta}{\partial t} + (\boldsymbol{U} \cdot \nabla)\theta = \kappa\nabla^2\theta, \tag{5}$$

where $\boldsymbol{U}$ is the velocity vector, p is the pressure, ρ_0 is the constant mean density, ν is the kinematic viscosity, and g is the gravitational acceleration. The streamwise, vertical, and spanwise directions are represented by x, y, and z, respectively, and the velocity components in these directions are U, V, and W. The gravity acts in the negative y direction. The origin of the coordinate system is located at the center of the computational domain. The unit vector in the y direction is $\boldsymbol{e}_y$. The scalar θ, defined by $\theta = -(\rho - \rho_0)/\rho_0$, represents minus the fractional density deviation (or the fractional specific volume deviation) [17]. The governing equations are numerically integrated from the initial states in the computational domain which is periodic in the horizontal (x and z) directions. At the upper and lower boundaries ($y = \pm L_y/2$), the impermeability condition is used for V and zero-flux conditions are used for U, W, and θ following Smyth [25].

The initial velocity profiles are generated by superimposing fluctuating components onto the mean velocity profile. The initial mean streamwise velocity profile is given by

$$U = \frac{U_0}{2}\tanh\left(\frac{2y}{h_0}\right), \tag{6}$$

where U_0 is the initial velocity difference and h_0 is the initial vorticity thickness defined by $h_0 = U_0/(\partial U_0/\partial y)_{\max}$. The initial vertical and spanwise mean velocities are 0. The velocity fluctuations are generated by a diffusion process which converts random noise into fluctuations that possess certain required length scales [28]. Statistically homogeneous and isotropic fluctuations are added to the mean velocity profile in the shear layer. The characteristic length and initial rms velocity fluctuations are $0.25h_0$ and $0.01U_0$, respectively. For the initial scalar field, the following profile is used without any scalar fluctuations:

$$\theta = \frac{\theta_0}{2}\tanh\left(\frac{2y}{h_0}\right), \tag{7}$$

where θ_0 is the difference in θ between the upper and lower sides of the mixing layer.

TABLE I. Physical and computational parameters of the DNS. The displayed turbulence characteristics are from the centerline.

Run	Re6Ri0	Re6Ri2	Re6Ri4	Re9Ri0	Re9Ri2	Re9Ri4	Re12Ri8
Re	600	600	600	900	900	900	1200
Ri	0	0.02	0.04	0	0.02	0.04	0.08
Pr	1	1	1	1	1	1	1
λ_x/h_0	1.34	1.35	1.32	1.06	1.09	0.94	0.70
η/h_0	0.053	0.057	0.057	0.038	0.043	0.042	0.034
L_O/h_0		2.93	1.07		2.44	1.14	0.41
λ_x/η	25.6	23.8	23.1	27.7	25.6	22.1	20.6
L_O/η		51.6	18.9		57.2	26.8	12.1
$\Delta x/\eta$	1.3	1.2	1.2	1.8	1.6	1.6	2.0
$\Delta y/\eta$	1.1	1.0	1.0	1.5	1.3	1.3	1.6
Re_λ	160	134	124	190	160	120	101
Re_b		192	51		220	80	28

The size of the computational domain is $L_x \times L_y \times L_z = 22.0\pi h_0 \times 17.5\pi h_0 \times 11.0\pi h_0$. For better statistical convergence, we use a larger computational domain in the x and z directions than in previous DNS [17] so that a large number of large-scale structures are contained in the computations. The large domain is also useful for reducing the unphysical effects of the periodicity on the flow development [29]. Recent DNS of temporally evolving mixing layers also used the domain size comparable to the present DNS [30]. When the governing equations are nondimensionalized by U_0, h_0, and θ_0, three nondimensional parameters appear in the equations: the Reynolds number $\mathrm{Re} = U_0 h_0/\nu$, the Prandtl number $\mathrm{Pr} = \nu/\kappa$, and the bulk Richardson number $\mathrm{Ri} = g\theta_0 h_0/U_0^2$. The DNS are performed for seven different sets of Ri and Re at a constant $\mathrm{Pr} = 1$ as summarized in Table I. The DNS results are presented with time t nondimensionalized by the reference time $T_{\mathrm{ref}} = h_0/U_0$. The same computational domain with the same grid points is used in all simulations.

The governing equations are solved by using a finite-difference method for spatial discretization and a third-order Runge-Kutta method for temporal advancement. The continuity and momentum equations are solved by using a fractional step method. The DNS code has been developed from those codes used in our previous studies [31–33]. Fully conservative fourth-order and second-order central-difference schemes [34] are used for spatial discretization in the horizontal and vertical directions, respectively. The Poisson equation for pressure is solved by using the Bi-CGSTAB method [35]. The computational domain is represented by $N_x \times N_y \times N_z = 1024 \times 650 \times 512$ computational grid points. The grid is equidistant in the x and z directions. In the y direction, a fine grid is used near the center of the mixing layer, and the grid is stretched near the vertical boundaries. The minimum resolution in the y direction is $0.056h_0$ at $y = 0$, and the maximum resolution is $0.21h_0$ at $y = \pm L_y/2$, which is far from the mixing layers. The resolutions are compared with the Kolmogorov scale on the centerline in Table I, and are small enough to capture the small-scale fluctuations.

III. TEMPORAL DEVELOPMENT OF MIXING LAYERS

We calculate the statistics from an instantaneous field by taking the average on an x-z plane at each vertical location; this averaged value is denoted by $\langle\ \rangle$. We here present the temporal variations of the various length scales which characterize the stably stratified mixing layer [17].

The momentum thickness δ_U is defined by

$$\delta_U = \int_{-L_y/2}^{L_y/2} \frac{(U_1 - \langle U\rangle)(\langle U\rangle - U_2)}{(U_0)^2} dy. \tag{8}$$

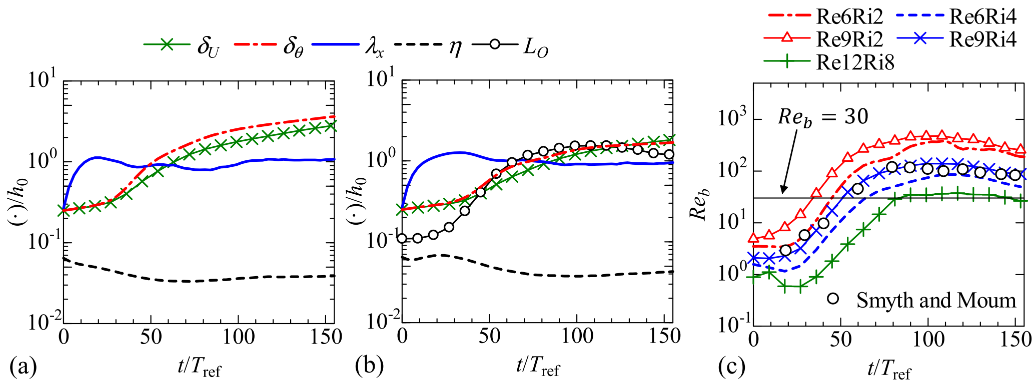

FIG. 1. Temporal variation of length scales of stably stratified mixing layers for (a) Re9Ri0 and (b) Re9Ri4. (c) Temporal variation of the buoyancy Reynolds number on the centerline compared with the DNS by Smyth and Moum [17].

Here, U_1 and U_2 are the values of $\langle U \rangle$ at $y = L_y/2$ and $-L_y/2$, respectively. Similarly, the thickness related to the mean scalar profile δ_θ is defined by

$$\delta_\theta = \int_{-L_y/2}^{L_y/2} \frac{(\theta_1 - \langle\theta\rangle)(\langle\theta\rangle - \theta_2)}{(\theta_0)^2} dy, \tag{9}$$

where θ_1 and θ_2 are the values of $\langle\theta\rangle$ at $y = L_y/2$ and $-L_y/2$, respectively. The Taylor microscale based on the ith – component of the velocity is defined by $\lambda_i = \sqrt{\langle u_i^2 \rangle / \langle (\partial u_i/\partial x_i)^2 \rangle}$ (with no summation on i), where $u_i = U_i - \langle U_i \rangle$ is the velocity fluctuation. Two important length scales can be defined in stably stratified turbulence based on the kinetic energy dissipation rate $\langle\varepsilon\rangle = 2\nu\langle S_{ij}S_{ij}\rangle$ [17]: the Kolmogorov scale $\eta = (\nu^3/\langle\varepsilon\rangle)^{1/4}$ and the Ozmidov scale $L_O = (\langle\varepsilon\rangle/N^3)^{1/2}$, where N is the buoyancy frequency given by $N = (g\langle\partial\theta/\partial y\rangle)^{1/2}$. Figures 1(a) and 1(b) show the evolution of these length scales on the centerline for (a) nonstratified and (b) stratified cases. The stratified mixing layer begins to develop three-dimensional instabilities from its initial state as the large scales are influenced by buoyancy. Then δ_U and δ_θ rapidly increase at $t/T_{\mathrm{ref}} \approx 40$, where turbulence begins to be generated through the KH instability. The figures show that the mixing layer thickness is reduced by the stratification. At the final stage, turbulence is suppressed by buoyancy even at small scales as L_O decreases while η increases with time [17]. This final stage appears for $t/T_{\mathrm{ref}} \gg 155$, which is not included in the present DNS. The various length scales at $t/T_{\mathrm{ref}} = 150$ in all simulations are summarized in Table I, where we can confirm that in the present DNS L_O is much larger than η.

The ratio between L_O and η is related to the buoyancy Reynolds number as

$$\mathrm{Re}_b = \left(\frac{L_O}{\eta}\right)^{4/3} = \frac{\langle\varepsilon\rangle}{\nu N^2}. \tag{10}$$

The time development of the buoyancy Reynolds number is shown in Fig. 1(c). The profiles are quite similar to those in the previous DNS by Smyth and Moum [17] for a stratified mixing layer at similar Re_b. The values of Re_b at $t/T_{\mathrm{ref}} = 150$ are given in Table I. Re_b exceeds the critical value of 30 [17,36] so that three-dimensional small-scale turbulence exists in all the simulations for $\mathrm{Ri} = 0.02$ and $\mathrm{Ri} = 0.04$. For $\mathrm{Ri} = 0.08$, Re_b is close this critical value. Figure 2 shows the temporal evolution of the gradient Richardson number on the centerline:

$$\mathrm{Ri}_g = \frac{g\langle\partial\theta/\partial y\rangle}{\langle\partial U/\partial y\rangle^2}. \tag{11}$$

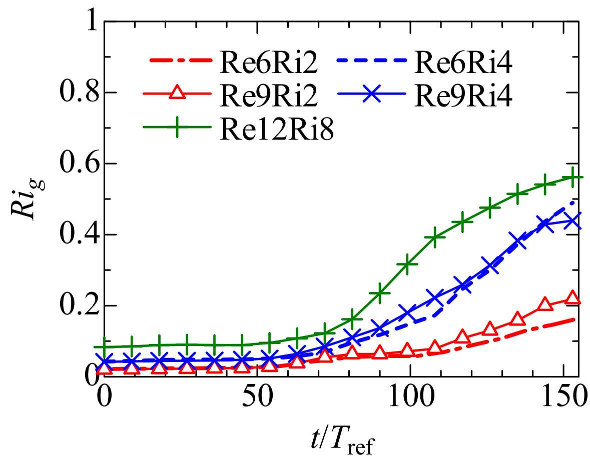

FIG. 2. Temporal variation of gradient Richardson number.

With the development of the mixing layers, Ri_g increases and the maximum value at $t/T_{\mathrm{ref}} = 150$ is 0.55 in the present DNS.

Figure 3 shows the vertical profiles of the mean streamwise velocity $\langle U \rangle$, streamwise velocity variance $\langle u^2 \rangle$, mean scalar $\langle \theta \rangle$, and scalar variance $\langle \theta'^2 \rangle$ at $t/T_{\mathrm{ref}} = 150$, where $\theta' = \theta - \langle \theta \rangle$ is the scalar fluctuation. The profiles in the nonstratified cases are similar to the previous DNS studies of temporally evolving mixing layers [37,38]. The suppression of the mixing layer thickness by the stratification is also found in these vertical profiles as confirmed by the wider profiles in the nonstratified case in Fig. 3. In addition, the values of the turbulent velocity fluctuations and the scalar fluctuations are seen to be significantly reduced by the stratification. Figure 4 visualizes, in the stratified mixing layer, the small-scale eddy structures based on the second invariant of the velocity gradient tensor $Q = (\omega_i \omega_i - 2S_{ij}S_{ij})/4$. As expected from the large Re_b, we can find small-scale eddies which look similar to those in the nonstratified mixing layers [39].

IV. T/NT INTERFACES IN STRATIFIED MIXING LAYERS

A. Detection of T/NT interfaces

We investigate the flows near the T/NT interface from snapshots at $t/T_{\mathrm{ref}} = 150$ for each of the DNS. The turbulent region in the stratified mixing layers is detected by thresholding the vorticity

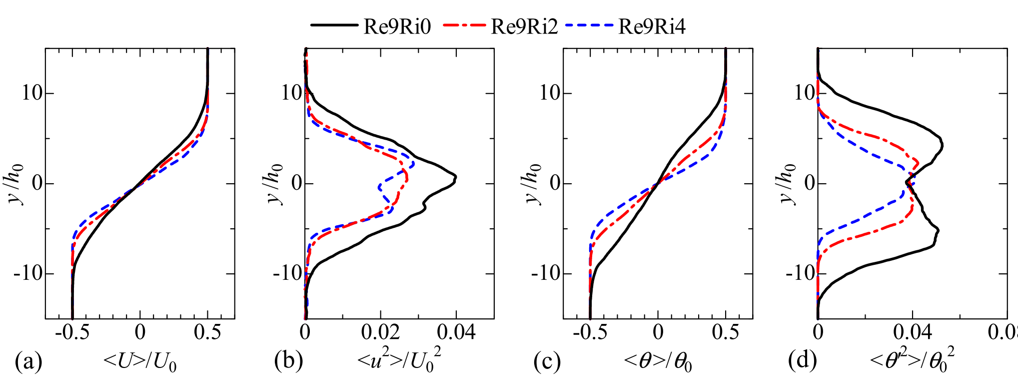

FIG. 3. Vertical profiles of (a) mean streamwise velocity $\langle U \rangle$, (b) streamwise velocity variance $\langle u^2 \rangle$, (c) mean scalar $\langle \theta \rangle$, and (d) scalar variance $\langle \theta'^2 \rangle$ at $t/T_{\mathrm{ref}} = 150$ ($\mathrm{Re} = 900$).

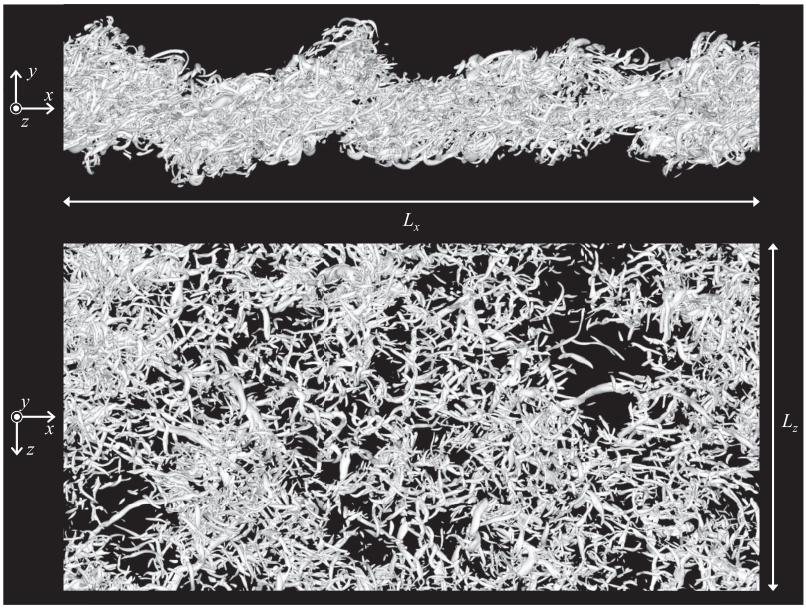

FIG. 4. Side and top views of small-scale eddy structures in the stratified mixing layer (Re9Ri4). The isosurface of the second invariant of the velocity gradient tensor $Q/\langle\omega^2/2\rangle_C = 1$ is visualized in the figure.

magnitude $|\boldsymbol{\omega}|$ as in the experimental studies of gravity currents [13]. Because the stratification is localized in the mixing layer and the density is essentially constant outside the turbulent region, internal gravity waves, which transport vorticity, cannot propagate outward. Therefore, unlike in stratified shear flows with constant ambient density gradients [40], we can detect the turbulent region with vorticity rather than potential vorticity [41]. The turbulent region is defined as the region with $|\boldsymbol{\omega}| \geqslant \omega_{th}$. We determined ω_{th} as $0.04\langle|\boldsymbol{\omega}|\rangle_C$, where the subscript C refers the value on the centerline. Taveira *et al.* [10] showed that when the turbulent volume is plotted as a function of the threshold, there exists a plateau for a wide range of the threshold and that the threshold value from this plateau can be effectively used for detecting the turbulent region. We confirmed that the present thresholds are in this plateau for all cases. This was also confirmed in the nonstratified mixing layer in a previous paper of ours [32]. The T/NT interface is detected by the isosurface of $|\boldsymbol{\omega}| = \omega_{th}$, which is located in the interface layer. As in our previous DNS of the nonstratified mixing layer [32], ω_{th} is small enough for the isosurface to be located close to the outer edge of the T/NT interface layer, and we refer to this isosurface as the *irrotational boundary*.

First we computed the probability density function (pdf) of the vertical height Y_I of the irrotational boundary from $y = 0$, as shown in Fig. 5. The effect of buoyancy is to decrease the height as Ri is increased, as seen in Fig. 5(a). The interface height is then normalized by the two length scales which characterize the thickness of the mixing layer: (b) the momentum thickness δ_U and (c) the thickness of the mean scalar profile δ_θ. We can see that the profiles collapse well using δ_U for normalization. The orientation of the irrotational boundary is given by its unit normal, $\boldsymbol{n} = (n_x, n_y, n_z) = -\nabla\omega^2/|\nabla\omega^2|$. Figure 6 gives the joint pdf of n_x and n_y computed from the irrotational boundary locations of the upper interface, where n_z is related to n_x and n_y by $|n_z| = \sqrt{1-(n_x^2+n_y^2)}$. The pdf for the stratified case shows significant peaks for $n_y \approx 1$, indicating that most interfaces have normals oriented in the vertical direction. In contrast, the interfaces in the nonstratified cases often face more in the streamwise direction, represented by large values of both $|n_x|$ and $|n_y|$. Figure 7 visualizes the isosurface of the vorticity magnitude used for detecting the T/NT interface in the nonstratified and stratified cases. The stable stratification is seen to cause the interface shape to have less structure, which is also reflected in the interface geometry statistics in Fig. 5(a). In particular, the small-scale

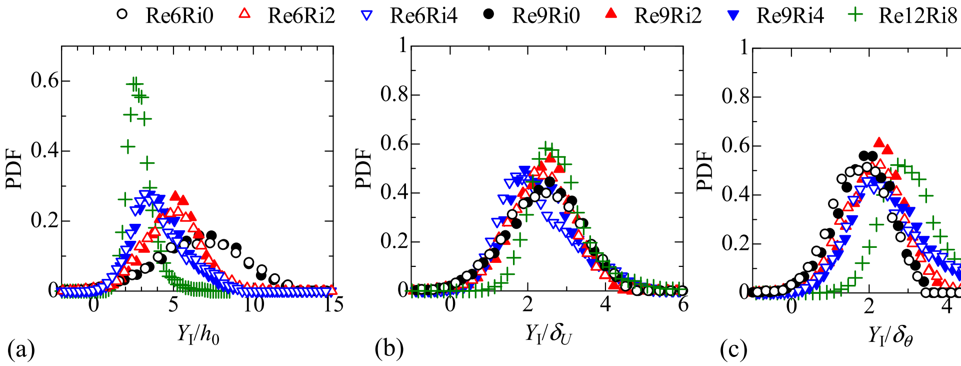

FIG. 5. Probability density function of the irrotational boundary height normalized by (a) the initial vorticity thickness h_0, (b) the momentum thickness δ_U, and (c) the thickness of the mean scalar profile δ_θ.

structures in the stratified case are not as significant as in the nonstratified case. The thresholds of the vorticity isosurface are slightly different in the stratified and nonstratified cases. However, we have confirmed, through visual tests, that the observed differences between the stratified and nonstratified cases are not due to the choice of the threshold. These results for the interface geometry indicate that stratification suppresses the turbulence development by reducing the surface area, as in the case of gravity currents [13].

B. Turbulence characteristics near the T/NT interface

The statistical properties near the T/NT interface are investigated using the statistics conditioned on the distance from the irrotational boundary [43]. The conditional statistics are calculated as a function of the local coordinate ζ_I, which is taken from the irrotational boundary in the boundary normal direction $\boldsymbol{n}$. The procedure for computing the conditional statistics is the same as in our previous study [32]. The turbulent side is where ζ_I is negative. The conditional statistics are presented with ζ_I normalized as $\zeta_\mathrm{I}/\eta_\mathrm{C}$, where η_C is the centerline value of the Kolmogorov scale.

Figure 8 shows the conditional mean vorticity magnitude and kinetic energy dissipation rate as functions of $\zeta_\mathrm{I}/\eta_\mathrm{C}$. For both stratified and nonstratified cases, these quantities show a sharp jump

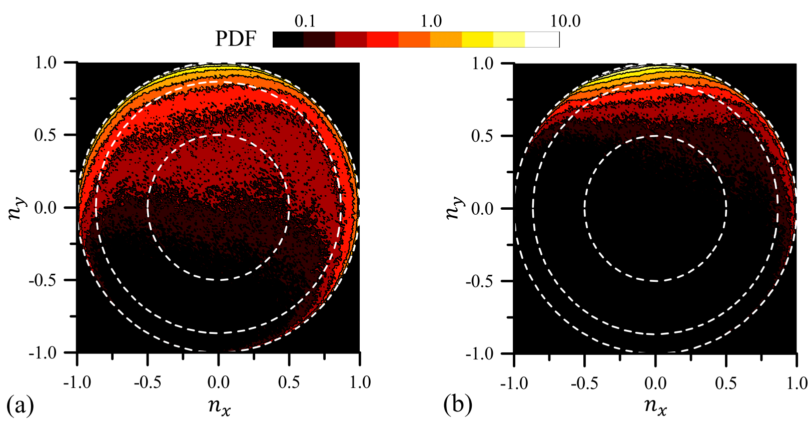

FIG. 6. Joint probability density functions (pdf) of streamwise and vertical components (n_x and n_y) of the boundary unit normal vector $\boldsymbol{n} = (n_x, n_y, n_z)$ for (a) Re9Ri0 and (b) Re9Ri4. The joint pdf is calculated from the upper T/NT interface. Three white broken lines indicate $\cos\theta \equiv |n_z| = \sqrt{1-(n_x^2+n_y^2)}$ for $\theta = 30^\circ, 60^\circ$ and 90° (from the inner line toward the outer line), where θ is the angle between $\boldsymbol{n}$ and the spanwise (z) direction.

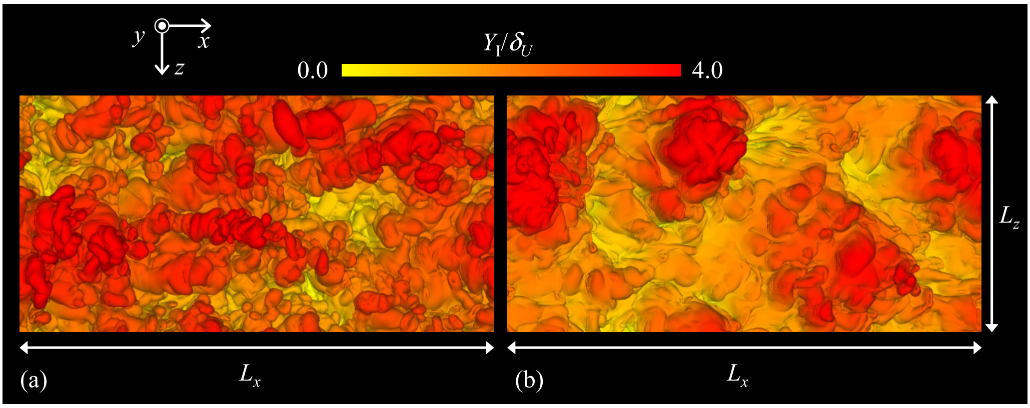

FIG. 7. Visualization of the irrotational boundary (the vorticity magnitude isosurface) in (a) nonstratified mixing layer (Re9Ri0) and (b) stratified mixing layer (Re9Ri4). The color shows the interface height from the centerline.

across the T/NT interface. The vorticity reaches the turbulent core value at $\zeta_I \approx -15\eta_C$, and the thickness of the T/NT interface layer is hardly modified by the effects of buoyancy. As mentioned above, the isosurface of $|\boldsymbol{\omega}| = \omega_{th}$ ($\zeta_I = 0$) is located near the outer edge of the T/NT interface layer. Thus, we can identify the T/NT interface layer in $-15\eta_C \leqslant \zeta_I \leqslant 0$. The insets in the figure compare the plots in the nonstratified cases with the DNS results of a spatially evolving mixing layer [42]. Both temporal and spatial simulations of mixing layers give similar conditional profiles of vorticity and kinetic energy dissipation rate. In the gravity current studied by Krug *et al.* [13], the normalized dissipation rate decreases with increasing Ri in the stratified flows. Similarly, it is decreased by the stratification in the stratified mixing layers in this study.

The enstrophy is governed by the following equation in the stratified flow:

$$\frac{D\omega^2/2}{Dt} = \omega_i S_{ij}\omega_j + \nu\nabla^2(\omega^2/2) - \nu\nabla\omega_i \cdot \nabla\omega_i + g\omega_i\varepsilon_{ij2}G_j\,. \tag{12}$$

The first term on the right-hand side is the production P_ω, the second is the viscous diffusion D_ω, the third is the viscous dissipation rate ε_ω, and the last term is the baroclinic torque B_ω. Figures 9(a)

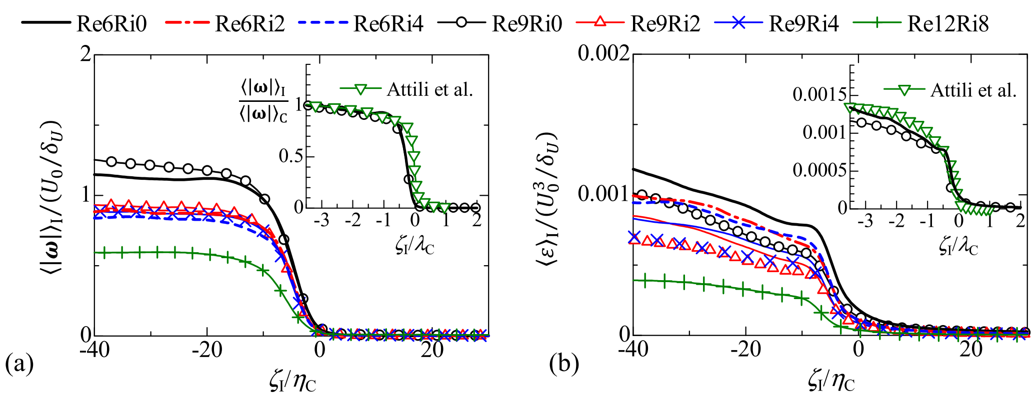

FIG. 8. Conditional averages of (a) vorticity magnitude $|\boldsymbol{\omega}|$ and (b) kinetic energy dissipation rate ε. The insets show the profiles in the nonstratified cases with the interface coordinate normalized by the centerline Taylor microscale $\lambda_C = (\lambda_x + \lambda_y + \lambda_z)/3$ compared with the DNS results in a spatially evolving mixing layer of Attili *et al.* [42]. In the inset of panel (a) the vorticity magnitude is normalized by the mean vorticity magnitude in the turbulent core region $\langle|\boldsymbol{\omega}|\rangle_C$.

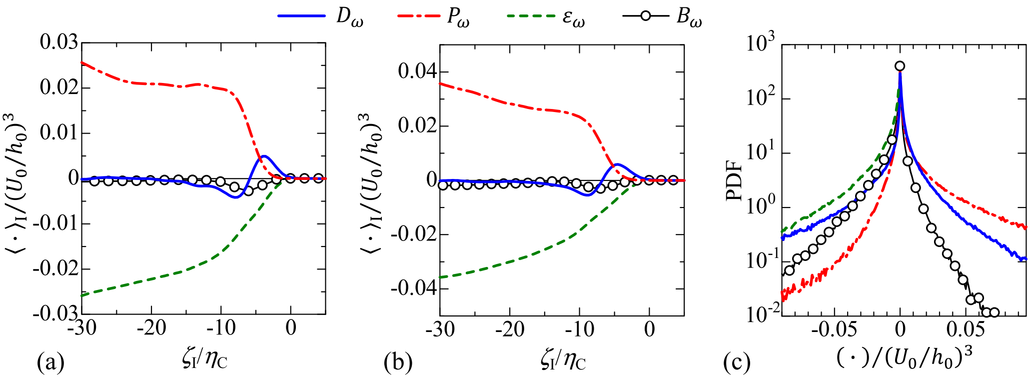

FIG. 9. Conditional enstrophy budgets for (a) Re9Ri4 and (b) Re12Ri8. (c) Conditional pdf of the enstrophy transport equation near the T/NT interface at $\zeta_\mathrm{I} = -8\eta_\mathrm{C}$ in Re9Ri4.

and 9(b) shows the conditional enstrophy budgets for Re9Ri4 and Re12Ri8, which are very similar to the budgets for the nonstratified mixing layers studied by previous DNS [32]. At the outer edge of the turbulent region, viscous diffusion makes a larger contribution than the production term. The width of the turbulent region with $\langle D_\omega \rangle_\mathrm{I} > \langle P_\omega \rangle_\mathrm{I}$ is $4.5\eta_\mathrm{C}$ for Re8Ri4 and $5.1\eta_\mathrm{C}$ for Re12Ri8. This width is related to the viscous superlayer thickness [44]. Thus the layer structure of the interface is almost independent of the stratification: The viscous superlayer with the thickness $\approx 5\eta_\mathrm{C}$ is formed at the outer edge of the interfacial layer, while the turbulent sublayer with the thickness $\approx 10\eta_\mathrm{C}$ appears between the viscous superlayer and the turbulent core region. These thicknesses agree well with the DNS results for nonstratified jets [8,9]. The baroclinic torque $\langle B_\omega \rangle_\mathrm{I}$ is close to 0, but has small negative value near the T/NT interface. The propagation velocity of the enstrophy isosurface, which is defined by $(D\omega^2/Dt)/|\nabla\omega^2|$, was investigated in the gravity current [13], where the T/NT interface was detected by the enstrophy isosurface. Their results also showed that at the outer edge of the T/NT interface, the enstrophy grows by the viscous effects and the mean contribution of the baroclinic torque is very small. The conditional pdf of each term in Eq. (12) is shown in Fig. 9(c) for $\zeta_\mathrm{I} = -8\eta_\mathrm{C}$ in Re9Ri4. Although the baroclinic torque cannot be neglected, especially in causing the decrease in the enstrophy near the interface, the probability for large negative B_ω is much smaller than that for large negative ε_ω.

Figures 10(a) and 10(b) give the conditional mean profiles of scalar θ and scalar dissipation rate $\chi = \kappa \nabla\theta \cdot \nabla\theta$ for the upper interface. We find the significant influence of buoyancy on the active

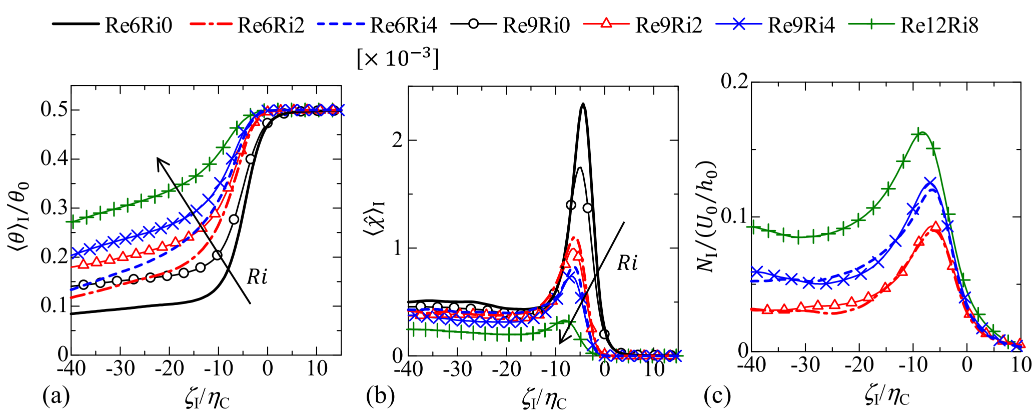

FIG. 10. Conditional mean profiles of (a) scalar θ, (b) scalar dissipation rate $\hat{\chi} = (h_0^2/\mathrm{RePr}\theta_0^2)\nabla\theta \cdot \nabla\theta$, and (c) local buoyancy frequency $N_\mathrm{I} = \sqrt{g\langle\partial\theta/\partial y\rangle_\mathrm{I}}$.

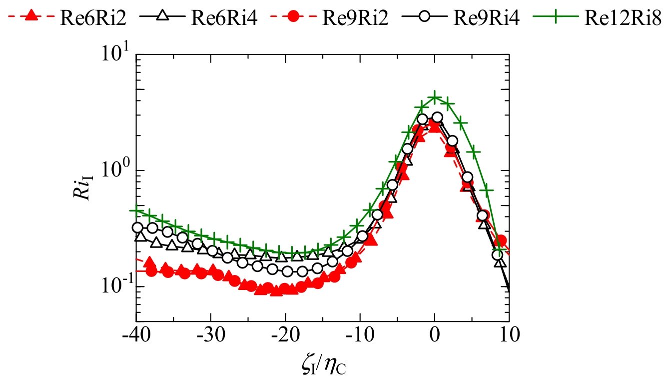

FIG. 11. Local Richardson number $\mathrm{Ri_I}$ across the T/NT interface.

scalar θ near the interface. The jump in $\langle\theta\rangle_\mathrm{I}$ across the interface decreases as Ri increases, consistent with the decrease in the conditional scalar gradient. This suggests that buoyancy also should act to reduce χ near the T/NT interface, which is seen to be the case in the figure. This effect is similar for $\mathrm{Re} = 600$ and 900 but depends on Ri. We can define the local buoyancy frequency near the T/NT interface as $N_\mathrm{I} = \sqrt{g\langle\partial\theta/\partial y\rangle_\mathrm{I}}$, which characterizes the strength of the stratification [45]. Figure 10(c) gives the normalized buoyancy frequency $\hat{N}_\mathrm{I} = \sqrt{\mathrm{Ri}\langle\partial\hat{\theta}/\partial\hat{y}\rangle_\mathrm{I}}$ ($\hat{\theta} = \theta/\theta_0, \hat{y} = y/h_0$) for the stratified cases. Because of the sharp jump in θ across the interface, the scalar gradient $\nabla\theta$ tends to be perpendicular to the interface [30]. Thus, as buoyancy causes the normal to the T/NT interface to be in the vertical direction, it does the same for $\nabla\theta$. Because of a large vertical scalar gradient in the T/NT interface, $\hat{N}_\mathrm{I}$ becomes large and the effects of the stratification are expected to be larger here than in the turbulent core region, as confirmed by the peak in $\hat{N}_\mathrm{I}$ in the interface layer. In the nonturbulent region, θ is constant and the buoyancy frequency approaches 0. The local buoyancy frequency in the gravity current [13] also exhibited a peak value in the interface layer, and the peak value increased with Ri. A similar tendency can be found in the stratified mixing layers. Furthermore, the present results show that the local buoyancy frequency near the T/NT interface is quite similar for $\mathrm{Re} = 600$ and 900. Figure 11 shows the local Richardson number near the T/NT interface, defined by $\mathrm{Ri_I} = N_\mathrm{I}^2/S_\mathrm{I}^2$, where $S_\mathrm{I} = \langle\partial U/\partial y\rangle_\mathrm{I}$ characterizes the local mean vertical shear near the interface. $\mathrm{Ri_I}$ increases in the T/NT interface layer and reaches the maximum at the outer edge of the T/NT interface layer ($\zeta_\mathrm{I} = 0$), where the stratification becomes strong compared with the local mean shear. A similar profile was found in the gravity current [13], where the maximum $\mathrm{Ri_I}$ was $\approx$0.1. In the present mixing layers, $\mathrm{Ri_I}$ reaches $\approx$3–5, as the stratification is stronger than in the gravity current.

Figure 12(a) shows, near the T/NT interface, the Kolmogorov and Ozmidov scales, defined by the local values of mean kinetic energy dissipation rate and buoyancy frequency as $\eta = (\nu^3/\langle\varepsilon\rangle_\mathrm{I})^{1/4}$ and $L_O = (\langle\varepsilon\rangle_\mathrm{I}/N_\mathrm{I}^3)^{1/2}$, respectively. The Ozmidov scale has a negative bump in the T/NT interface layer because of large N_I in this region, indicating that stratification has more effect on the smaller scales in the T/NT interface layer than in the turbulent core region. It reaches less than 10 times of η in the T/NT interface layer, and thus the dissipation range is strongly influenced by stratification there. It is also found that Ri has a larger influence on L_O than does Re, while the opposite is true for η. Figure 12(b) shows the local buoyancy Reynolds number computed from the local Ozmidov and Kolmogorov scales. Because of the decrease in L_O in the T/NT interface layer, the buoyancy Reynolds number also decreases significantly and becomes of the order of 10. The buoyancy Reynolds number in the turbulent core region is nearly constant. In the nonturbulent region, it becomes large again because the stratification is very weak, as confirmed with small N_I in Fig. 10(c). The dependence of Re_b on Re is small in the T/NT interface layer as Ri appears to determine Re_b in this region (note that $\mathrm{Pr} = 1$). Re_b becomes minimum near the location where the

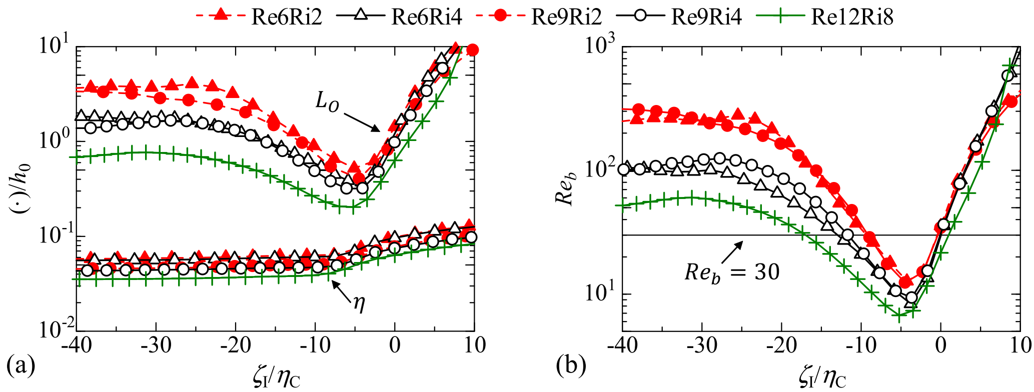

FIG. 12. (a) Conditional profiles of Kolmogorov and Ozmidov scales (η and L_O) across the T/NT interface. (b) Buoyancy Reynolds number Re_b across the T/NT interface.

scalar gradient is large. A peak of the scalar gradient appears near the boundary between the turbulent sublayer and the viscous superlayer, which is located at $\zeta_I \approx -5\eta_C$ [32]. Therefore, stratification has most significant influence at this location in the interface layer.

V. STRATIFICATION EFFECTS ON SMALL-SCALE TURBULENCE DYNAMICS NEAR THE T/NT INTERFACE

A. Alignments of small-scale structures

We investigate the buoyancy effects on the strain/vorticity and strain/scalar-gradient interactions near the T/NT interface. These interactions are represented by the production terms for $\omega^2/2$ and χ in Eqs. (1) and (2), respectively. The contributions of the eigenvalues, s_i, of the strain-rate tensor significantly depend on the alignments among $\boldsymbol{\omega}$, $\boldsymbol{G}$, and $\boldsymbol{e}_i$. The effective strains acting on the vorticity and the scalar gradient can be defined as follows [25]:

$$\alpha_\omega = \frac{\omega_i S_{ij} \omega_j}{\omega^2} = s_i(\boldsymbol{e}_i \cdot \hat{\boldsymbol{\omega}})^2, \tag{13}$$

$$\gamma_\chi = -\frac{G_i S_{ij} G_j}{G^2} = -s_i(\hat{\boldsymbol{G}} \cdot \boldsymbol{e}_i)^2. \tag{14}$$

Here α_ω and γ_χ are the production rates of enstrophy and of the scalar dissipation, respectively [18]. Note that positive α_ω signifies vortex stretching, while positive γ_χ signifies the compression of the scalar gradient. Therefore, positive values of the effective strains contribute to the amplification of enstrophy and of scalar dissipation rate. Figure 13 shows the conditional mean plots of α_ω and γ_χ. The effects of stratification are seen to be strong in the T/NT interface layer, while the plots tend to collapse onto one curve in the turbulent core region. Smyth also showed that in the turbulent core region in stratified mixing layers, γ_χ is reduced by stratification when the buoyancy Reynolds number is small [25]. A similar trend can be found in the T/NT interface layer, where Re_b sharply drops.

Figure 14 compares the pdfs of the cosine of the alignment angle of the vorticity and the strain-rate eigenvectors $|\hat{\boldsymbol{\omega}} \cdot \boldsymbol{e}_i|$ for the stratified and nonstratified cases. The stratification changes the alignments for $\boldsymbol{e}_1$ and $\boldsymbol{e}_3$ near the T/NT interface, while they are quite similar for both stratified and nonstratified cases in the turbulent core regions. However, the stratification hardly changes the alignment for $\boldsymbol{e}_2$ even near the T/NT interface. The stratification causes the vorticity vector to misalign with $\boldsymbol{e}_1$, which makes the vortex stretching less effective. Furthermore, the compressible strain more effectively acts on the vorticity near the T/NT interface in the stratified flow. The pdfs of $|\hat{\boldsymbol{G}} \cdot \boldsymbol{e}_i|$ are shown in Fig. 15 and are compared with the DNS results near the centerline in the

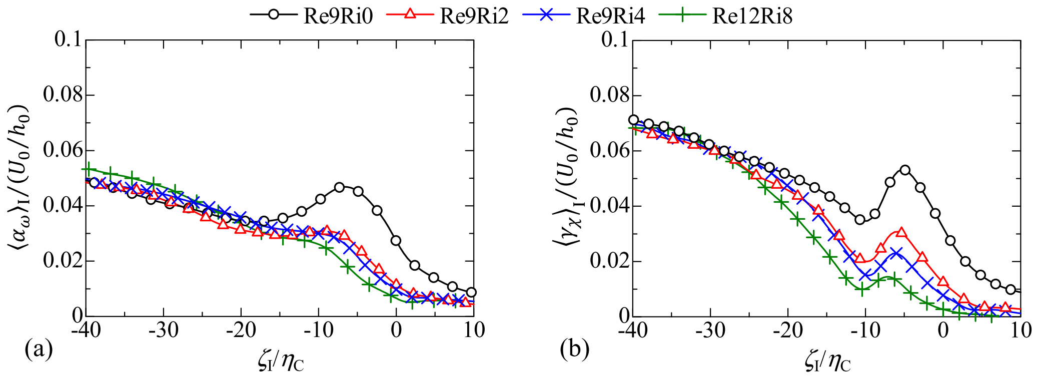

FIG. 13. Conditional profiles of (a) effective extensive strain acting on vorticity vector $\alpha_\omega = \omega_i S_{ij}\omega_j/(\omega_k\omega_k)$ and (b) effective compressive strain acting on scalar gradient $\gamma_\chi = -G_i S_{ij} G_j/(G_k G_k)$.

stratified mixing layer at high Re_b by Smyth [25]. Similar to $|\hat{\boldsymbol{\omega}} \cdot \boldsymbol{e}_i|$, the alignment is modified by buoyancy for the extensive and compressive eigenvectors near the T/NT interface. Compared with the nonstratified case, the extensive strain s_1 more efficiently acts on the scalar gradient near the T/NT interface in the stratified flows and vice versa for the compressive strain s_3. We have also confirmed that the alignment statistics are similar between Re9Ri4 and Re9Ri2 (not shown here),

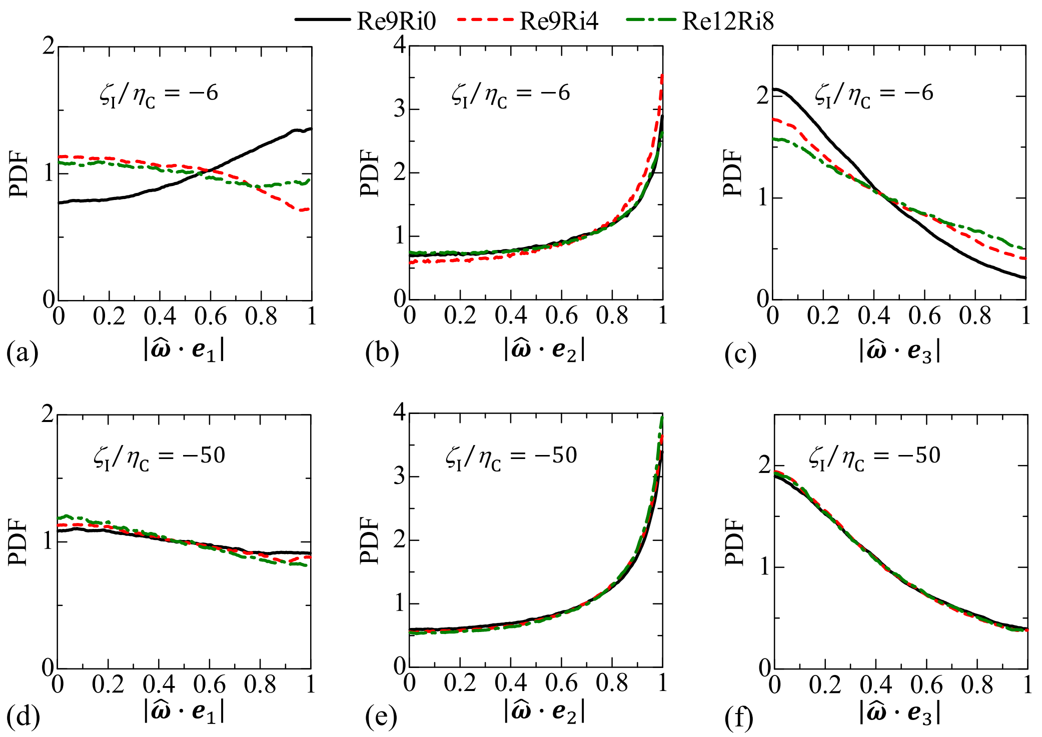

FIG. 14. Conditional pdf of the cosine of the alignment angles of the vorticity vector and the strain-rate eigenvectors near the T/NT interface ($\zeta_\mathrm{I} = -6\eta_\mathrm{C}$) for (a) the extensive strain $\boldsymbol{e}_1$, (b) intermediate strain $\boldsymbol{e}_2$, and (c) compressive strain $\boldsymbol{e}_3$. (d)–(f) Conditional pdf as in panels (a)–(c) obtained in the turbulent core region ($\zeta_\mathrm{I} = -50\eta_\mathrm{C}$).

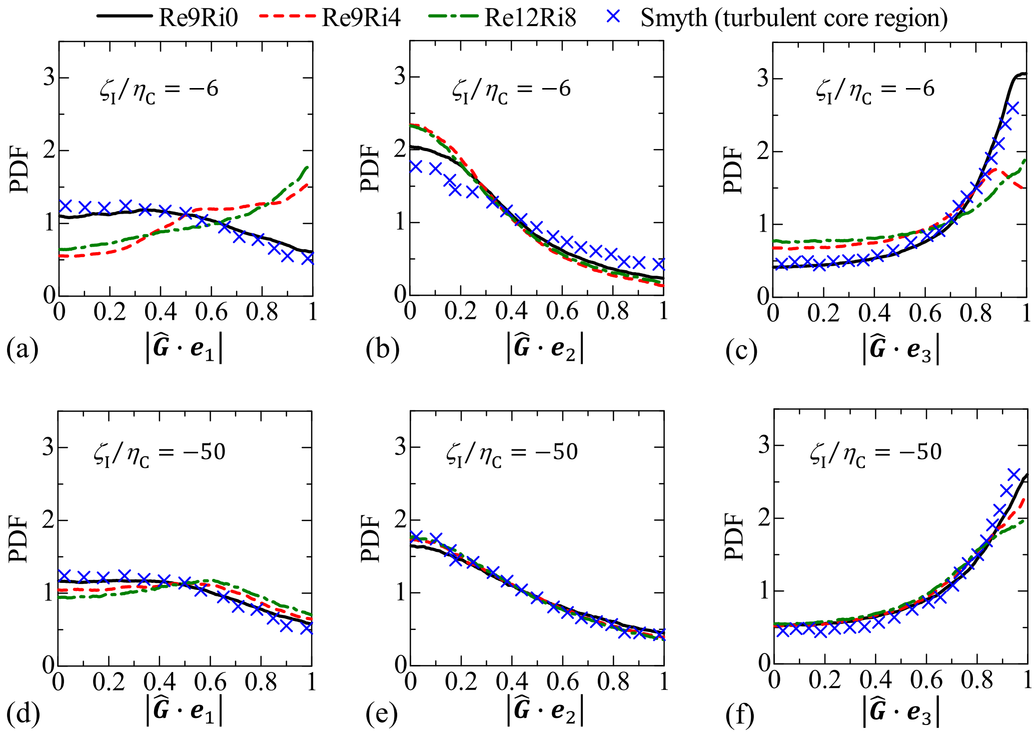

FIG. 15. Conditional pdf of the cosine of the alignment angles of the scalar gradient and the strain-rate eigenvectors near the T/NT interface ($\zeta_I = -6\eta_C$) for (a) the extensive strain $\boldsymbol{e}_1$, (b) intermediate strain $\boldsymbol{e}_2$, and (c) compressive strain $\boldsymbol{e}_3$. (d)–(f) Conditional pdf as in panels (a)–(c) obtained in the turbulent core region ($\zeta_I = -50\eta_C$). The present results are compared with the turbulent core region of the stratified mixing layer at high buoyancy Reynolds number in the DNS by Smyth [25].

independently of the two Re cases. The stratification makes the effective strains α_ω and γ_χ small via these changes in the alignments near the interface.

The comprehensive set of DNS by Smyth showed that stratification changes the alignment statistics of $\boldsymbol{G}$ and $\boldsymbol{e}_i$ as Re_b decreases to less than $\mathrm{Re}_b = O(10)$ [25], where the stratification was found to cause $\boldsymbol{e}_2$ to misalign with $\boldsymbol{G}$. This tendency cannot be seen near the T/NT interface in Fig. 15(b) although Re_b becomes small here. This raises a possibility that there is a different mechanism in which the stratification changes the alignment near the T/NT interface. In nonstratified jets, the strain strongly depends on a velocity field near the interface [20]. For turbulent fluids moving towards the T/NT interface, $\boldsymbol{e}_1$ and $\boldsymbol{e}_3$ are in the interface tangential and normal directions, respectively. Opposite tendencies were found in the turbulent fluids moving away from the interface: $\boldsymbol{e}_1$ and $\boldsymbol{e}_3$ are normal and tangential to the T/NT interface, respectively. For both cases, the vorticity and scalar-gradient vectors near the interface are tangential and perpendicular to the T/NT interface, respectively. It is useful to define $\Delta\boldsymbol{U}$ [20] as the fluid velocity in relation to the irrotational boundary movement. The velocity of the irrotational boundary movement [11] is the sum of the fluid velocity $\boldsymbol{U}_0$ on the irrotational boundary and the boundary propagation velocity $\boldsymbol{U}_\mathrm{p}$, where $\boldsymbol{U}_\mathrm{p}$ is given by $\boldsymbol{U}_\mathrm{p} = [(D\omega^2/Dt)/|\nabla\omega^2|]\boldsymbol{n}$. Then, $\Delta\boldsymbol{U} = \boldsymbol{U} - \boldsymbol{U}_0 - \boldsymbol{U}_\mathrm{p}$. The interface normal component can be obtained by $\Delta U_N = \Delta\boldsymbol{U}\cdot\boldsymbol{n}$, where a turbulent fluid with positive ΔU_N is approaching the irrotational boundary. Figure 16 shows the conditional mean value of ΔU_N for the higher Re cases. Stratification makes $\langle\Delta U_N\rangle_\mathrm{I}$ smaller in the turbulent region, indicating that the turbulent motion toward the T/NT interface is suppressed by stratification. The large-scale flow characteristics, such as mean flows, have a strong influence on ΔU_N [20]. Note that the interface normal direction is

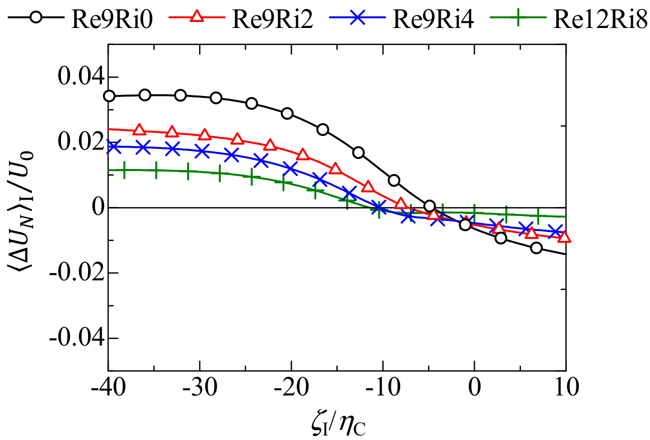

FIG. 16. Conditional mean velocity relative to the irrotational boundary in the boundary normal direction.

frequently parallel to the vertical direction in the stratified cases. Therefore, the suppression of the large-scale vertical motion by the buoyancy can be related to the decrease in $\langle \Delta U_N \rangle_{\mathrm{I}}$. Because the small scales are not independent of the large scales in turbulent flows, the buoyancy effects on the large scales can be reflected in the small-scale characteristics. This buoyancy effect on the turbulent fluid motion modifies the direction near the interface of $\boldsymbol{e}_1$ and $\boldsymbol{e}_3$ but not $\boldsymbol{e}_2$ [20], resulting in the changes in the alignment statistics for $\boldsymbol{e}_1$ and $\boldsymbol{e}_3$ observed in the T/NT interface layer.

B. Structures of large scalar dissipation-rate regions

Various studies of the turbulent mixing of passive scalars have shown that a region with large scalar dissipation rate appears as a sheetlike structure [46,47]. It has also been shown that this structure is well approximated by a one-dimensional (1D) diffusion-layer model [48]. At steady state, the model implies that the thinning effect of compressive strain balances with the thickening effect of molecular diffusion. Therefore, at steady state, the characteristic thickness of the diffusion layer is given by $\lambda_{\mathrm{1D}} = \sqrt{2\kappa/\gamma}$, where γ is a compressive strain rate. The sheetlike structures frequently appear along the T/NT interface because of a large scalar gradient in the T/NT interface layer [30,32,42]; furthermore they are expected to affect the conditional mean profiles of the scalar field. According to Kothnur and Clemens [48], a characteristics thickness of the sheetlike structures, λ_χ, near the T/NT interface is estimated using the location of 20% of the peak in $\langle \chi \rangle_{\mathrm{I}}$ as in Fig. 17. This thickness is given by $\lambda_\chi = 1.77\lambda_{\mathrm{1D}}$ in the one-dimensional diffusion-layer model [48]. The

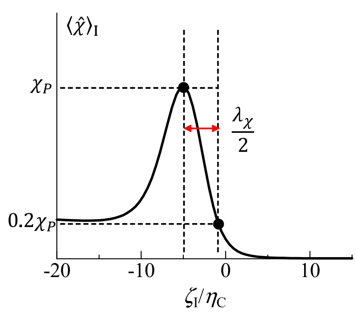

λ_χ calculated from $\langle \hat{\chi} \rangle_{\mathrm{I}}$ and 1D model

Case	$\langle \hat{\chi} \rangle_{\mathrm{I}}$	1D model
Re6Ri0	7.2η (0.28λ)	8.7η
Re6Ri2	7.2η (0.30λ)	11.0η
Re6Ri4	6.9η (0.30λ)	12.5η
Re9Ri0	9.1η (0.33λ)	9.4η
Re9Ri2	8.0η (0.31λ)	11.2η
Re9Ri4	8.3η (0.37λ)	13.2η
Re12Ri8	9.6η (0.46λ)	18.5η

FIG. 17. Comparison between the thickness of large scalar dissipation layer in $\langle \chi \rangle_{\mathrm{I}}$ near the T/NT interface observed in the DNS and the one-dimensional diffusion layer model (1D model) [48].

diffusion layer model is used for estimating λ_χ, where the effective strain rate $\langle\gamma_\chi\rangle_I$ at the location of the peak in $\langle\chi\rangle_I$ is used as γ in $\lambda_\chi = 1.77\sqrt{2\kappa/\gamma}$. The table in Fig. 17 compares λ_χ computed from the conditional mean scalar dissipation rate with λ_χ computed from the diffusion-layer model. λ_χ is found to be less than the interface thickness $\approx 15\eta_C$, and of the order of the Kolmogorov scale. The 1D steady model based on the effective strain rate predicts λ_χ for the nonstratified cases fairly well, while it overestimates λ_χ in the stratified cases. The assumption of the compressive strain acting on the diffusion layer appears valid near the T/NT interface in the nonstratified cases as confirmed from a peak in the pdf at $|\hat{\boldsymbol{G}} \cdot \boldsymbol{e}_3| = 1$ [Fig. 15(c)]. In the stratified cases, however, the extensive strain-rate eigenvector $\boldsymbol{e}_1$ near the T/NT interface frequently aligns with $\hat{\boldsymbol{G}}$ and the diffusion layer model is invalid because the compressive strain does not sustain the layer.

VI. CONCLUDING REMARKS

Temporally evolving stably stratified mixing layers, where the stratification is localized in the shear layers, are simulated using DNS. The stratification effects are investigated near the T/NT interface in these mixing layers whose buoyancy Reynolds number at the centerline is large enough for small-scale turbulence to exist.

First, buoyancy effects are found in the interface geometry: In the stratified cases, the T/NT interface appears closer to the centerline, and a large part of the T/NT interface has its normal near the vertical direction. These geometrical changes decrease the surface area of the interface, reducing the total entrainment rate, as has been confirmed in previous studies of gravity currents [13]. The structure of the T/NT interface is similar in stratified and nonstratified flows. A viscous superlayer exists at the outer edge of the turbulent region and an adjacent layer, the turbulent sublayer, appears between the viscous superlayer and the turbulent core region. The thicknesses of these layers are about 4–5η_C and 10η_C, respectively, which agree with the previous DNS results of nonstratified jets [8,9].

The stratification was found to be locally strengthened near the T/NT interface, as evidenced by the large scalar gradient in the vertical direction, and resulting in a sharp decrease in the Ozmidov scale in the T/NT interface layer. This is reflected in the local buoyancy Reynolds number Re_b, which is decreased to $\mathrm{Re}_b \approx 10$ near the T/NT interface even though $\mathrm{Re}_b = O(10^2)$ in the turbulent core region. Thus buoyancy effects on the small-scale turbulence dynamics are significant in the T/NT interface layer. We found that the production rates of the enstrophy and the scalar dissipation rate, which arise from the strain/vorticity and strain/scalar-gradient interactions, are indeed decreased in the T/NT interface layer. This is because the stratification modifies the alignments among the vorticity, scalar gradient, and strain-rate eigenvectors. A possible explanation was given for the influence of buoyancy on these alignment statistics based on the relation between the strain-rate field and the turbulent motion in relation to the T/NT interface. It has been confirmed that the effective strain rate tends to be large for the turbulent fluids approaching the T/NT interface in nonstratified jets [20]. The suppression of the vertical motions by buoyancy reduces the turbulent fluid motions approaching the T/NT interface, resulting in reduced effective strain rates acting on the vorticity and the scalar gradient. Although the thickness of the scalar dissipation profile near the interface agrees with a one-dimensional diffusion layer model [48] in the nonstratified cases, this model poorly predicts the layer thickness near the interface in the stratified cases; in these cases the assumption of the compressive strain acting in the scalar gradient direction is no longer valid near the T/NT interface.

The present results show that even if the buoyancy Reynolds number is large in the localized turbulent region, which is often observed in geophysical flows, the turbulence in the outer edges, where mass, energy, and scalar exchanges with the exterior flow occur, is strongly influenced by the stable stratification.

ACKNOWLEDGMENTS

The numerical simulations presented in this manuscript were carried out on a high-performance computing system (NEC SX-ACE) in the Japan Agency for Marine-Earth Science and Technology.

The authors would like to thank Dr. R. Onishi and Dr. K. Matsuda for their help in the numerical simulations on SX-ACE. This work was supported by JSPS KAKENHI Grants No. 16K18013 and No. 25289030 and by the US Office of Naval Research via Grant No. N00014-15-1-2248.

---

[1] S. A. Thorpe, The near-surface ocean mixing layer in stable heating conditions, J. Geophys. Res. **83**, 2875 (1978).

[2] L. Mahrt, Stratified atmospheric boundary layers, Boundary-Layer Meteorol. **90**, 375 (1999).

[3] R. S. Lindzen, Turbulence and stress owing to gravity wave and tidal breakdown, J. Geophys. Res. **86**, 9707 (1981).

[4] C. B. da Silva, J. C. R. Hunt, I. Eames, and J. Westerweel, Interfacial layers between regions of different turbulence intensity, Annu. Rev. Fluid Mech. **46**, 567 (2014).

[5] C. B. da Silva and R. R. Taveira, The thickness of the turbulent/nonturbulent interface is equal to the radius of the large vorticity structures near the edge of the shear layer, Phys. Fluids **22**, 121702 (2010).

[6] S. Corrsin and A. L. Kistler, Free-stream boundaries of turbulent flows, NACA Technical Report No. TN-1244, 1033 (1955).

[7] J. Westerweel, C. Fukushima, J. M. Pedersen, and J. C. R. Hunt, Mechanics of the Turbulent-Nonturbulent Interface of a Jet, Phys. Rev. Lett. **95**, 174501 (2005).

[8] R. R. Taveira and C. B. da Silva, Characteristics of the viscous superlayer in shear free turbulence and in planar turbulent jets, Phys. Fluids **26**, 021702 (2014).

[9] M. van Reeuwijk and M. Holzner, The turbulence boundary of a temporal jet, J. Fluid Mech. **739**, 254 (2014).

[10] R. R. Taveira, J. S. Diogo, D. C. Lopes, and C. B. da Silva, Lagrangian statistics across the turbulent-nonturbulent interface in a turbulent plane jet, Phys. Rev. E **88**, 043001 (2013).

[11] M. Holzner and B. Lüthi, Laminar Superlayer at the Turbulence Boundary, Phys. Rev. Lett. **106**, 134503 (2011).

[12] J. Philip, C. Meneveau, C. M. de Silva, and I. Marusic, Multiscale analysis of fluxes at the turbulent/non-turbulent interface in high Reynolds number boundary layers, Phys. Fluids **26**, 015105 (2014).

[13] D. Krug, M. Holzner, B. Lüthi, M. Wolf, W. Kinzelbach, and A. Tsinober, The turbulent/non-turbulent interface in an inclined dense gravity current, J. Fluid Mech. **765**, 303 (2015).

[14] D. Krug, M. Holzner, B. Lüthi, M. Wolf, W. Kinzelbach, and A. Tsinober, Experimental study of entrainment and interface dynamics in a gravity current, Exp. Fluids **54**, 1 (2013).

[15] I. P. D. De Silva, H. J. S. Fernando, F. Eaton, and D. Hebert, Evolution of Kelvin-Helmholtz billows in nature and laboratory, Earth Planet. Sci. Lett. **143**, 217 (1996).

[16] J. N. Moum, Efficiency of mixing in the main thermocline, J. Geophys. Res. **101**, 12057 (1996).

[17] W. D. Smyth and J. N. Moum, Length scales of turbulence in stably stratified mixing layers, Phys. Fluids **12**, 1327 (2000).

[18] A. Tsinober, *An Informal Conceptual Introduction to Turbulence* (Springer, Berlin, 2009).

[19] P. J. Diamessis and K. K. Nomura, Interaction of vorticity, rate-of-strain, and scalar gradient in stratified homogeneous sheared turbulence, Phys. Fluids **12**, 1166 (2000).

[20] T. Watanabe, Y. Sakai, K. Nagata, Y. Ito, and T. Hayase, Vortex stretching and compression near the turbulent/nonturbulent interface in a planar jet, J. Fluid Mech. **758**, 754 (2014).

[21] W. T. Ashurst, A. R. Kerstein, R. M. Kerr, and C. H. Gibson, Alignment of vorticity and scalar gradient with strain rate in simulated Navier-Stokes turbulence, Phys. Fluids **30**, 2343 (1987).

[22] Z. S. She, E. Jackson, and S. A. Orszag, Structure and dynamics of homogeneous turbulence: Models and simulations, Proc. Royal Soc. London, Ser. A **434**, 101 (1991).

[23] O. R. H. Buxton and B. Ganapathisubramani, Amplification of enstrophy in the far field of an axisymmetric turbulent jet, J. Fluid Mech. **651**, 483 (2010).

[24] C. H. Gibson, Fossil temperature, salinity, and vorticity turbulence in the ocean, Marine Turbulence **28**, 221 (1980).

[25] W. D. Smyth, Dissipation-range geometry and scalar spectra in sheared stratified turbulence, J. Fluid Mech. **401**, 209 (1999).
[26] C. Staquet and J. J. Riley, A numerical study of a stably-stratified mixing layer, in *Selected Papers from the Sixth Symposium on Turbulent Shear Flows* (Springer, Berlin, 1989), pp. 381–397.
[27] K. A. Brucker and S. Sarkar, Evolution of an initially turbulent stratified shear layer, Phys. Fluids **19**, 105105 (2007).
[28] A. Kempf, M. Klein, and J. Janicka, Efficient generation of initial and inflow conditions for transient turbulent flows in arbitrary geometries, Flow Turbul. Combust. **74**, 67 (2005).
[29] P. A. Davidson, *Turbulence: An Introduction for Scientists and Engineers* (Oxford University Press, Oxford, UK, 2004).
[30] M. Gampert, J. Boschung, F. Hennig, M. Gauding, and N. Peters, The vorticity versus the scalar criterion for the detection of the turbulent/non-turbulent interface, J. Fluid Mech. **750**, 578 (2014).
[31] T. Watanabe, Y. Sakai, K. Nagata, Y. Ito, and T. Hayase, Enstrophy and passive scalar transport near the turbulent/non-turbulent interface in a turbulent planar jet flow, Phys. Fluids **26**, 105103 (2014).
[32] T. Watanabe, Y. Sakai, K. Nagata, Y. Ito, and T. Hayase, Turbulent mixing of passive scalar near turbulent and non-turbulent interface in mixing layers, Phys. Fluids **27**, 085109 (2015).
[33] T. Watanabe, C. B. da Silva, Y. Sakai, K. Nagata, and T. Hayase, Lagrangian properties of the entrainment across turbulent/non-turbulent interface layers, Phys. Fluids **28**, 031701 (2016).
[34] Y. Morinishi, T. S. Lund, O. V. Vasilyev, and P. Moin, Fully conservative higher order finite difference schemes for incompressible flow, J. Comput. Phys. **143**, 90 (1998).
[35] H. A. Van der Vorst, Bi-CGSTAB: A fast and smoothly converging variant of Bi-CG for the solution of nonsymmetric linear systems, SIAM J. Sci. Statist. Comput. **13**, 631 (1992).
[36] S. Almalkie and S. M. de Bruyn Kops, Kinetic energy dynamics in forced, homogeneous, and axisymmetric stably stratified turbulence, J. Turbulence **13**, N29 (2012).
[37] M. M. Rogers and R. D. Moser, Direct simulation of a self-similar turbulent mixing layer, Phys. Fluids **6**, 903 (1994).
[38] C. Pantano, S. Sarkar, and F. A. Williams, Mixing of a conserved scalar in a turbulent reacting shear layer, J. Fluid Mech. **481**, 291 (2003).
[39] M. Tanahashi, S. Iwase, and T. Miyauchi, Appearance and alignment with strain rate of coherent fine scale eddies in turbulent mixing layer, J. Turbulence **2**, N6 (2001).
[40] A. M. Abdilghanie and P. J. Diamessis, The internal gravity wave field emitted by a stably stratified turbulent wake, J. Fluid Mech. **720**, 104 (2013).
[41] T. Watanabe, J. J. Riley, S. M. de Bruyn Kops, P. J. Diamessis, and Q. Zhou, Turbulent/non-turbulent interfaces in wakes in stably stratified fluids, J. Fluid Mech. **797**, R1 (2016).
[42] A. Attili, J. C. Cristancho, and F. Bisetti, Statistics of the turbulent/non-turbulent interface in a spatially developing mixing layer, J. Turbulence **15**, 555 (2014).
[43] D. K. Bisset, J. C. R. Hunt, and M. M. Rogers, The turbulent/non-turbulent interface bounding a far wake, J. Fluid Mech. **451**, 383 (2002).
[44] R. Jahanbakhshi, N. S. Vaghefi, and C. K. Madnia, Baroclinic vorticity generation near the turbulent/non-turbulent interface in a compressible shear layer, Phys. Fluids **27**, 105105 (2015).
[45] G. R. Spedding, Anisotropy in turbulence profiles of stratified wakes, Phys. Fluids **13**, 2361 (2001).
[46] K. A. Buch and W. J. A. Dahm, Experimental study of the fine-scale structure of conserved scalar mixing in turbulent shear flows. Part 1. Sc $\gg$ 1, J. Fluid Mech. **317**, 21 (1996).
[47] L. K. Su and N. T. Clemens, The structure of fine-scale scalar mixing in gas-phase planar turbulent jets, J. Fluid Mech. **488**, 1 (2003).
[48] P. S. Kothnur and N. T. Clemens, Effects of unsteady strain rate on scalar dissipation structures in turbulent planar jets, Phys. Fluids **17**, 125104 (2005).